Interplay of superfluorescence and incoherent processes in multilevel systems

Fritz Haake and Reinhard Reibold
Fachbereich Physik, Universität Essen—Gesamthochschule, D-4300 Essen, Germany
(Received 30 January 1984)

We investigate the interaction of spontaneous collective radiation with incoherent pumping and damping mechanisms. In discussing a recent experiment of two-color superfluorescence, we allow for two optically active level pairs which have their upper level in common. Satisfactory agreement with the experimental results is achieved.

I. INTRODUCTION

The wealth of experimental information on superfluorescence has been increased impressively by the recent observation of collective spontaneous radiation of O_2^- centers in KCl crystals.[1] This experiment deserves special interest for a variety of reasons. One is the joint appearance of two pulses, one red and one yellow, in many events. A strong coupling between the two pulses in a pair is indicated by their perfect synchronization. Furthermore, the excited state of the O_2^- center from which the alternative transitions originate is not populated instantaneously. Rather it is filled by incoherent leakage from an initially populated level higher up in energy, the corresponding time constant being small but not negligible compared to the duration of the pulses. Finally, the lower levels in the two transitions are part of an incoherent damping cascade. For sufficiently high temperature and for low O_2^--center concentration this damping cuts off the collective radiation. Even for temperatures and densities allowing for the generation of superfluorescent pulses, the damping remains effective in determining the relative intensities of the two pulses in a pair.

The complications incurred in discussing the experiment mentioned are intriguing indeed. Instead of initially inverted two-level systems we have to treat collections of systems with at least four levels. Rather than facing a monochromatic pulse emerging from an effectively frictionless medium we are confronted with two pulses of different colors which interact with each other and compete with incoherent pumping and damping mechanisms.

We propose to study, in the present paper, the effects of pumping and damping on the dynamics and the statistics of superfluorescence, as well as the peculiarities of two-color superfluorescence. Before confronting all of these complications together (Sec. V) we shall discuss them in sequence one at a time. Section II is devoted to the interplay of pumping and superfluorescence. We consider systems with three levels, the uppermost of which is populated initially, while the lower two are the optically active ones. Radiation can arise only after some population has leaked incoherently from the uppermost level into the intermediate one. In Sec. III we turn to initially inverted two-level systems, allowing for the lower level to suffer incoherent depletion. The problem of two competing colors is taken up in Sec. IV. To account for two transitions we consider two pairs of levels with the upper level in common. The lower two levels are subjected to incoherent depletion.

Our methods will be very similar to those of Ref. 2. We shall not derive the Heisenberg equations which generalize the Maxwell-Bloch equations pertinent to two-level systems. The derivation involves no concepts other than the ones amply laid out in Ref. 2. The damping and noise terms showing up below can be established in a variety of equivalent and well-known ways.[3] We shall mostly use dimensionless variables based on units introduced in Ref. 2. In contrast to our previous work, here we use a retarded time coordinate, $(x,t)\rightarrow(x,t-x/c)$.

II. INCOHERENT PUMPING AND COLLECTIVE RADIATION

To study the effect of an incoherent pump mechanism[4] on the buildup of collective radiation we propose to consider a three-level system (Fig. 1). Initially, all atoms are assumed in the uppermost level, labeled as 4, while the radiatively active levels, 3 and 2, are empty, and all polarizations are zero. Following the preparation of that initial state the atoms start to fall incoherently into level 3, thus building up an inversion in the pair 3 and 2. Collective radiation due to cooperative transitions from level 3 to 2 can then start and continue until no atom is left in either level 4 or 3.

In the limit of an infinitely fast relaxation, $4\rightarrow3$, the model in question will describe superfluorescence from initially inverted two-level atoms. Here, we shall be interested in the change of the dynamical and statistical properties of the radiation as the "pumping" time τ_{43} becomes comparable with, or larger than, the time constant

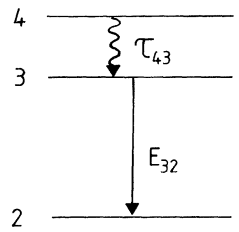

FIG. 1. Three-level system considered to discuss pumping and superfluorescence.

of the cooperative radiation, τ_{sf}.

For the sake of simplicity we assume the incoherent pumping $4\rightarrow 3$ to be due to a weak coupling of the atoms to some heat bath at low temperatures,

$$\hbar/\tau_{43} \ll k_B T \ll E_4 - E_3 , \tag{2.1}$$

with no resonance near $E_4 - E_3$. The pumping of level 3 is then Markovian in nature. The Heisenberg equations of motion read, with the dimensionless pumping rate $\gamma = \tau_{sf}/\tau_{43}$,

$$\begin{aligned}
&\frac{\partial}{\partial t} N_4 = -\gamma N_4 + \xi_4 , \\
&\frac{\partial}{\partial t} N_3 = -(R_{32}^{+} E_{32}^{+} + R_{32}^{-} E_{32}^{-}) + \gamma N_4 - \xi_4 , \\
&\frac{\partial}{\partial t} N_2 = +(R_{32}^{+} E_{32}^{+} + R_{32}^{-} E_{32}^{-}) , \\
&\frac{\partial}{\partial t} R_{32}^{\pm} = +(N_3 - N_2) E_{32}^{\mp} + \xi_{32}^{\pm} , \\
&\frac{\partial}{\partial x} E_{32}^{\mp} = R_{32}^{\pm} .
\end{aligned} \tag{2.2}$$

The quantum-noise fields ξ_4 and $\xi_{32}^{\pm}$ are independent, white, and Gaussian, and have zero means and the second moments

$$\begin{aligned}
&\langle \xi_{32}^{+} \xi_{32}^{+} \rangle = \langle \xi_{32}^{-} \xi_{32}^{-} \rangle = \langle \xi_{32}^{-} \xi_{32}^{+} \rangle = 0 , \\
&\langle \xi_4(x,t) \xi_4(x',t') \rangle = \langle \xi_{32}^{+}(x,t) \xi_{32}^{-}(x',t') \rangle \\
&\qquad = \frac{1}{N} \langle N_4(t) \rangle \gamma \delta(x - x') \delta(t - t') \\
&\qquad = \frac{1}{N} e^{-\gamma t} \gamma \delta(x - x') \delta(t - t') .
\end{aligned} \tag{2.3}$$

Apart from the irreversible terms, the Heisenberg equations (2.2) are the usual Maxwell-Bloch equations for unidirectional propagation of a plane-wave pulse generated by the level pair 3 and 2.[2] The pumping mechanism yields no upward transitions $3\rightarrow 4$ and does not explicitly affect the polarization $R_{32}^{\pm}$ except through a noise term in the low-temperature limit (2.1). The appearance of $\langle N_4 \rangle$ in the noise moments in (2.3) shows that we are dealing with a multiplicative stochastic process.

The initial state $|0\rangle$, with respect to which we shall have to evaluate expectation values, is the vacuum for the electromagnetic field and an eigenstate of the occupation number operators N_4, N_3, and N_2 with eigenvalues 1, 0, and 0, respectively,

$$\begin{aligned}
&E_{32}^{+}(x,0) |0\rangle = N_3(x,0) |0\rangle = N_2(x,0) |0\rangle = 0 , \\
&N_4(x,0) |0\rangle = 1 .
\end{aligned} \tag{2.4}$$

This initial state, in contrast to the one pertinent to superfluorescence from initially inverted two-level atoms, is not an unstable equilibrium state. Rather, the relaxation of the atoms out of level 4 would set in immediately even if the noise were neglected. However, in such a classical approximation Eqs. (2.2) would not yield radiation. Atoms leaked out of level 4 would accumulate in level 3 and stay there forever. It is this intermediate level, therefore, which corresponds to an unstable equilibrium. Collective radiation as the signature of the decay of the unstable equilibrium eventually sets in due to the noise source $\xi_{32}^{\pm}$.

We can find the radiation statistics in two steps. First, for the early stage during which the intensity is still weak, $\langle E_{32}^{-} E_{32}^{+} \rangle \ll 1$, we linearize the Heisenberg equations (2.2) and construct closed-form solutions. Then, once the fields have grown out of the noise-dominated regime we invoke the correspondence principle, i.e., drop the quantum-noise operators and treat the further dynamics classically. Since we assume $N \gg 1$, this classical regime begins long before the nonlinearity of Eqs. (2.2) becomes appreciable and lasts until most atoms settle in the final state, 2.

In contrast to the case of superfluorescence from initially inverted two-level atoms we have not found a special representation in which the dynamics looks classical from the beginning, all quantum effects being accounted for as initial uncertainties of $R_{32}^{\pm}$ and/or $E_{32}^{\pm}$.[2] This is because the unstable equilibrium is not realized initially, here, but is rather built up by pumping as the noise-induced decay is already taking place.

In the linear regime the occupation-number operators are immediately found as

$$\begin{aligned}
&N_4(x,t) = N_4(x,0) e^{-\gamma t} + \int_0^t dt' e^{-\gamma(t-t')} \xi_4(t') , \\
&N_3(x,t) = N_3(x,0) + N_4(x,0) - N_4(x,t) , \\
&N_2(x,t) = N_2(x,0) .
\end{aligned} \tag{2.5}$$

When inserting the inversion $N_3 - N_2$ from (2.5) into the Heisenberg equation for $R_{32}^{\pm}$ we neglect the noise term involving ξ_4. This is possible because $E_{32}^{\mp}$ is of first order in the noise $\xi_{32}^{\pm}$, while the product $\xi_4 E_{32}^{\mp}$ is of second order. Moreover, with respect to the initial state specified in (2.4) the initial operators $N_2(x,0)$, $N_3(x,0)$, and $N_4(x,0)$ can be replaced by the respective eigenvalues 0, 0, and 1. The coupled equations for the active polarization and the electric field then take the form, with the indices "23" dropped,

$$\frac{\partial}{\partial t} R^{\pm} = (1 - e^{-\gamma t}) E^{\mp} + \xi^{\pm} , \quad \frac{\partial}{\partial x} E^{\mp} = R^{\pm} . \tag{2.6}$$

In these linearized Heisenberg equations the pumping of level 3 appears as an imposed process.

Moreover, we could obviously interpret (2.6) as classical Langevin equations for complex classical stochastic fields $R(x,t) \hat{=} R^{+}(x,t)$ and $E(x,t) \hat{=} E^{-}(x,t)$, which are driven by the complex classical noise $\xi(x,t) \hat{=} \xi^{+}(x,t)$. The noise $\xi(x,t)$ is nonstationary, white, and Gaussian, and has zero mean and the second moment given in (2.3). The correlation functions

$$\langle E(x_1,t_1) \cdots E(x_n,t_n) E^{*}(x_n',t_n') \cdots E^{*}(x_1',t_1') \rangle$$

for this classical process are identical with the corresponding normally ordered correlation functions of the quantum operators, provided the classical analog of the quantum initial conditions (2.4) are used, i.e., $E(x,0) = R(x,0) = 0$.

The linearized equations (2.6) immediately yield to solution by Laplace transformation. The electric field operator comes out as

$$E^{\mp}(x,t)=\int_0^t dt'\int_0^x dx' I_0(2[(x-x')F(t,t')]^{1/2})\xi^{\pm}(x',t')+\int_0^x dx' I_0(2[(x-x')F(t,0)]^{1/2})R^{\pm}(x',0)$$
$$+\int_0^t dt'[x/F(t,t')]^{1/2} I_1(2[xF(t,t')]^{1/2})(1-e^{-\gamma t'})E^{\mp}(0,t')+E^{\mp}(0,t)\ , \tag{2.7}$$

where I_0 and I_1 are modified Bessel functions, and

$$F(t,t')=t-t'+(e^{-\gamma t}-e^{-\gamma t'})/\gamma\ . \tag{2.8}$$

The polarization $R^{\pm}(x,t)$ follows from (2.7) as the derivative of $E^{\mp}(x,t)$ with respect to x.

We shall not allow for external signals impinging on the atoms, and can thus set

$$E^{\mp}(0,t)=0 \tag{2.9}$$

in the result (2.9).

Were we dealing with an initial state of complete inversion of the active level pair, we would have $\langle N_4\rangle=0$ at all times and thus, due to (2.3), a vanishing noise strength. Only the second term in (2.7), the one well known to describe superfluorescence from two-level atoms, would thus survive. For the initial state defined in (2.4), however, this term does not contribute to expectation values of electric field operators and can therefore be dropped from (2.7).

With the electric field thus represented by the first term on the right-hand side in (2.7) we quickly find the dynamical and statistical behavior of the radiated electric field. Similar to the source $\xi^{\pm}$, the field $E^{\mp}$ has zero mean and Gaussian statistics. The mean radiation intensity at the right end of the active volume results from (2.4) and (2.7) as

$$I(t)=\langle E^{-}(1,t)E^{+}(1,t)\rangle$$
$$=\frac{\gamma}{N}\int_0^t dt' e^{-\gamma t'}[\{I_0(2[F(t,t')]^{1/2})\}^2$$
$$-\{I_1(2[F(t,t')]^{1/2})\}^2]\ , \tag{2.10}$$

and the higher-order intensity moments as

$$\langle E^{-}(1,t)^n E^{+}(1,t)^m\rangle=\delta_{nm}n!I(t)^n\ . \tag{2.11}$$

In the limit of very fast pumping, $\gamma\to\infty$, the intensity (2.10) reduces to

$$\lim_{\gamma\to\infty} I(t)=\frac{1}{N}\{[I_0(2\sqrt{t})]^2-[I_1(2\sqrt{t})]^2\}\ , \tag{2.12}$$

a result well known from two-level–atom superfluorescence. In fact, we can formally carry out that limit in (2.7) and obtain

$$\lim_{\gamma\to\infty} E^{\mp}(x,t)=\int_0^x dx' I_0(2[(x-x')]^{1/2}t)R^{\pm}_{\rm eff}(x',0)\ ,$$
$$R^{\pm}_{\rm eff}(x,0)=\int_0^\infty dt\,\xi^{\pm}(x,t) \tag{2.13}$$

as an effective initial polarization. The precise meaning of Eq. (2.13) is that it entails the correct $\gamma\to\infty$-limits for all electric field expectation values.

We gain more insight into the radiation statistics if we define, for the equivalent classical random process

$$E(x,t)=\int_0^x dx'\int_0^t dt' I_0(2[(x-x')F(t,t')]^{1/2})\xi(x',t')\ , \tag{2.14}$$

a passage time by

$$|E(1,t)|^2=I_{\rm ref}\ , \tag{2.15}$$

with a suitable reference intensity

$$1/N\ll I_{\rm ref}\lesssim 1\ . \tag{2.16}$$

Actually, the condition (2.14) does not determine a unique passage time. Owing to the white noise ξ, every trajectory (2.14) will, in fact, cross any reference threshold infinitely often. We expect all passages of one trajectory to cluster together in time relatively tightly, at least for reference intensities well above the noise-dominated regime, i.e., in the range (2.16). The time rate of change of the probability for finding the intensity above the reference level,

$$W(t)=\frac{d}{dt}\langle\Theta(|E(1,t)|^2-I_{\rm ref})\rangle\ , \tag{2.17}$$

where the average $\langle\ \rangle$ is one over the Gaussian white noise ξ with the second moments (2.3), should thus not be an absurd approximation of the probability density of, for instance, the first-passage time. Since the electric field vanishes initially and appears, in the linearized description in question, to be growing indefinitely, the function $W(t)$ is normalized to unity,

$$\int_0^\infty dt\,W(t)=1\ . \tag{2.18}$$

Every trajectory is thus assigned one effective passage through the reference level.

The Gaussian functional average in (2.17) is easily carried out and yields the simple result

$$W(t)=\frac{\dot{I}(t)I_{\rm ref}}{I(t)^2}\exp\left[-\frac{I_{\rm ref}}{I(t)}\right]\ , \tag{2.19}$$

where $I(t)$ is the mean intensity (2.10).

By inspecting the mean intensity (2.10) and the passage-time distribution (2.19) we can infer the following qualitative properties of the mean and the variance of the passage time. For fast pumping the mean passage time at finite γ is larger than the mean passage time at infinite γ, by roughly the pumping time $1/\gamma$, while the variance of the passage time is roughly independent of γ,

$$\left.\begin{aligned}\langle t\rangle_\gamma &\approx\langle t\rangle_\infty+1/\gamma\\ {\rm var}_\gamma(t) &\approx{\rm var}_\infty(t)\end{aligned}\right\}\ \text{for } 1/\gamma\lesssim(\langle t\rangle_\gamma)^{1/2}\ . \tag{2.20}$$

These results are intuitive since the pumping process enters the linearized equations of motion (2.6) as a deterministic effect.

In the limit of slow pumping, on the other hand, we have the crude asymptotic approximations

$$\left.\begin{array}{ll}\langle t\rangle_\gamma & \sim\gamma^{-1/2}\\ \langle t^2\rangle_\gamma & \sim\gamma^{-1}\end{array}\right\} \text{ for } 1/\gamma > \langle t\rangle_\gamma \,. \tag{2.21}$$

The estimates (2.20) and (2.21) are confined by the numerical results drawn from (2.10) and (2.19) which we display in Fig. 2.

The foregoing discussion of the early-stage linear regime should be complemented with an investigation of the subsequent nonlinear behavior. To that end we must solve the classical versions of the field equations (2.2) by numerical means. Statistical statements become possible once we have calculated a large number of solutions which represent, at early times, the Gaussian ensemble characteristic of the linear regime.

In order to construct the nonlinear trajectories with minimal labor we first calculate, for a fixed time t_0, the correlation functions

$$\langle E(x,t_0)E^*(x',t_0)\rangle \,,$$

$$\langle R(x,t_0)E^*(x',t_0)\rangle \,,$$

and

$$\langle R(x,t)R^*(x',t_0)\rangle$$

by using the linear result (2.14) and

$$R(x,t_0)=\partial E(x,t_0)/\partial x \,.$$

These correlation functions, together with

$$\langle N_3^2\rangle-\langle N_3\rangle^2=\langle N_4^2\rangle-\langle N_4\rangle^2=\frac{4}{N}(e^{-2\gamma t_0}-e^{-3\gamma t_0}) \,, \tag{2.22}$$

$$\langle N_2^2\rangle=0 \,,$$

and the first moments

$$\langle N_4\rangle=1-\langle N_3\rangle=e^{-\gamma t_0} \,, \tag{2.23}$$

$$\langle R\rangle=\langle E\rangle=\langle N_2\rangle=0 \,,$$

define a Gaussian ensemble at the time t_0. Actually, since the variances of the occupation numbers (2.22) are very much smaller than the ones of R and E we can, without noticeable error, regard N_3 and N_4 as sharp.

We have employed a random-number generator to produce, on a grid of points x_i, a set of configurations $R(x_i),E(x_i)$ corresponding to the Gaussian ensemble defined above. For each such configuration as a set of initial values at time t_0 we have integrated the classical versions of the nonlinear equations (2.2). Assuming the time t_0 to be sufficiently large for the fields E and R to have risen well above the noise-dominated regime, we have, in computing the nonlinear trajectories, neglected the noise forces ξ_4 and $\xi_{32}=\xi$.

The statistical results thus obtained are depicted, together with the corresponding ones of the linear analysis, in Fig. 3. The histograms show, for three values of γ, the delay times of the first pulse maxima. Each histogram represents an ensemble of 160 nonlinear trajectories. The smooth curves are the corresponding distributions (2.19), the reference intensities I_{ref} chosen such that the mean passage time agrees with the mean delay time (drawn from the histogram).

The agreement between the linear and the nonlinear results in Fig. 3 is a rather satisfactory one. There is, however, a slight tendency, as the pumping gets slower, of the linear result (2.19) to underestimate the delay-time fluctuations. This tendency is due to the fact that an increase of the pumping time tends to make the (nonlinear) pulses flatter in shape, as is illustrated, for the mean intensity, in Fig. 4.

III. INCOHERENT DAMPING AND COLLECTIVE RADIATION

We now investigate two-level superfluorescence as influenced by an incoherent depletion of the lower level. For the sake of simplicity we assume an initial state of complete inversion in the active level pair which we again label as 3 and 2. Imagining the depletion to be due to a low-temperature heat bath such that the depletion rate constant Γ of level 2 obeys

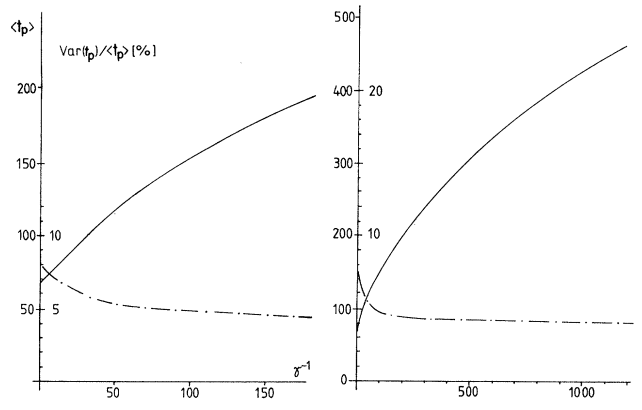

FIG. 2. Mean (solid line) and relative variance (dashed-dotted line) of the passage time as functions of the dimensionless pumping time derived from (2.19).

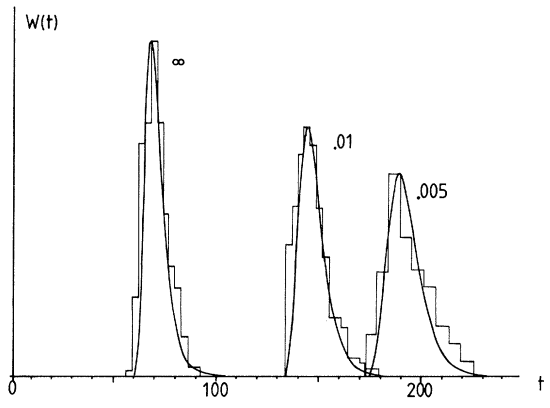

FIG. 3. Delay-time statistics for different values of the pumping rate ($\gamma=\infty$, 0.001, and 0.005). The histograms represent ensembles of 160 nonlinear trajectories, while the smooth distributions are calculated from (2.19).

$$\hbar\Gamma \ll k_B T \ll E_3 - E_2 \ , \tag{3.1}$$

we have the following Heisenberg equations of motion:

$$\begin{aligned}
&\frac{\partial}{\partial t} N_3 = -(R_{32}^{+} E_{32}^{+} + R_{32}^{-} E_{32}^{-}) \ , \\
&\frac{\partial}{\partial t} N_2 = -\frac{\partial}{\partial t} N_3 - \Gamma N_2 + \xi_2 \ , \\
&\frac{\partial}{\partial t} R_{32}^{\pm} = (N_3 - N_2) E_{32}^{\mp} - \tfrac{1}{2}\Gamma R_{32}^{\pm} + \xi_{32}^{\pm} \ , \\
&\frac{\partial}{\partial x} E_{32}^{\mp} = R_{32}^{\pm} \ .
\end{aligned} \tag{3.2}$$

The Gaussian-noise forces have zero means and strengths defined by

$$\begin{aligned}
&\langle \xi_2(x,t)\xi_2(x',t') \rangle = \frac{\Gamma}{N} \langle N_2(x,t) \rangle \delta(x-x')\delta(t-t') \ , \\
&\langle \xi_{32}^{+}(x,t)\xi_{32}^{-}(x',t') \rangle = \frac{\Gamma}{N} \langle N_3(x,t) \rangle \delta(x-x')\delta(t-t') \ .
\end{aligned} \tag{3.3}$$

All second-order noise correlations except the ones in (3.3) vanish.

The initial state $|0\rangle$ of the system is the vacuum for the electromagnetic field and the fully inverted state for all atoms. We therefore have

$$\begin{aligned}
&N_3(x,0)|0\rangle = |0\rangle \ , \\
&N_2(x,0)|0\rangle = R_{32}^{+}(x,0)|0\rangle = E_{32}^{+}(0,0)|0\rangle = 0 \ .
\end{aligned} \tag{3.4}$$

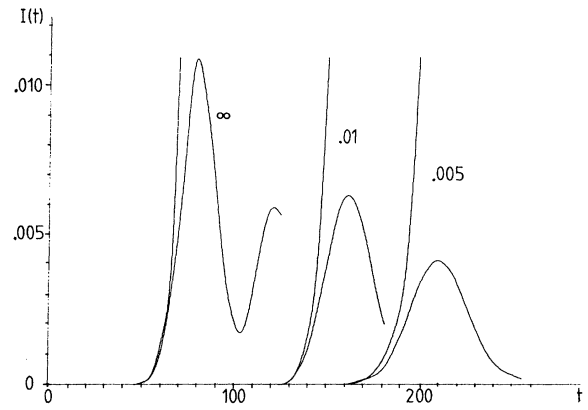

FIG. 4. Comparison of linear (diverging) and nonlinear (bounded) trajectories for the mean intensity at the end of the sample for various values of the pumping rate ($\gamma = \infty$, 0.01, and 0.005).

By assuming the limit of a high number density of atoms we provide the initial polarization with Gaussian statistics with

$$\langle 0 | R_{32}^{+}(x,0) R_{32}^{-}(x',0) | 0 \rangle = \frac{1}{N} \delta(x-x') \tag{3.5}$$

as the elementary correlation.

The damping mechanism can affect the radiation process quite drastically. In fact, the inequality

$$\frac{\partial}{\partial t} \int_0^1 dx \langle 0 | R_{32}^{+}(x,t) R_{32}^{-}(x,t) | 0 \rangle \leq \frac{\Gamma}{N} + (2-\Gamma) \int_0^1 dx \langle 0 | R_{32}^{+}(x,t) R_{32}^{-}(x,t) | 0 \rangle \ , \tag{3.6}$$

implied by (3.2), rules out the possibility of coherent amplification for sufficiently strong damping, $\Gamma \gtrsim 2$.

In the early-stage linear regime the equations of motion (3.2) simplify to (with all indices dropped)

$$\frac{\partial}{\partial t} R^{\pm} = E^{\mp} - \tfrac{1}{2}\Gamma R^{\pm} + \xi^{\pm} \ , \quad \frac{\partial}{\partial x} E^{\mp} = R^{\pm} \ . \tag{3.7}$$

Up to terms not contributing to normally ordered moments, we then find the electric field operator as the sum of two terms, one involving the initial polarization, the other proportional to the noise which accompanies the damping process,

$$E^{\mp}(x,t) = \int_0^t dt' e^{-(1/2)\Gamma(t-t')} \int_0^x dx' I_0(2[(x-x')(t-t')]^{1/2}) \xi^{\pm}(x',t') + e^{-(1/2)\Gamma t} \int_0^x dx' I_0(2[(x-x')t]^{1/2}) R^{\pm}(x',0) \ . \tag{3.8}$$

By using the initial condition (3.5) and the noise correlations (3.3) we find the mean intensity at the right end of the medium,

$$\begin{aligned}
I(t) &= \langle E^{-}(1,t) E^{+}(1,t) \rangle \\
&= \frac{1}{N} \left[1 + \int_0^t dt' e^{-\Gamma t'} I_1(2(t')^{1/2})^2 / t' \right] .
\end{aligned} \tag{3.9}$$

Obviously, $I(t)$ approaches a time-independent value $I(\infty)$ for $t \gg 1/\Gamma$. Individual intensity trajectories will, of course, not approach a constant limiting value, but rather they fluctuate randomly around $I(\infty)$. Physically, the saturation of $I(t)$ at large times represents a balance between energy dissipation into the heat bath and generation of radiation energy out of an effectively inexhaustible (due to the linear approximation!) reservoir. In the limit of a vanishing depletion rate constant Γ such a balance is not possible and the intensity found in the linear approximation must increase beyond all bounds as $t \to \infty$.

For strong damping we have $I(\infty) \ll 1$. The linear approximation then remains valid as long as the radiated energy is smaller than the initial atomic excitation energy, i.e., for $\int_0^t dt' I(t') < N$. This regime is customarily referred to as that of amplified spontaneous emission.[5]

In Fig. 5 we display the mean intensity $I(t)$ as calculated from (3.9) for various values of Γ. Rather modest values of Γ obviously suffice to reduce $I(t)$ drastically. In Fig. 6 we compare, again for various values of Γ, the mean intensities predicted by the linear theory and a numerically generated ensemble of nonlinear trajectories.

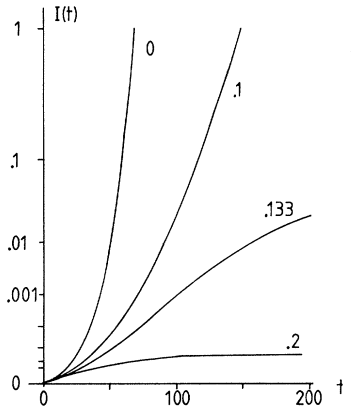

FIG. 5. Mean intensity (linear theory) for various values of the depletion rate Γ. Only for the strongest damping ($\Gamma=0.2$) is the stationary value $I(\infty)$ reached within the scope of the diagram.

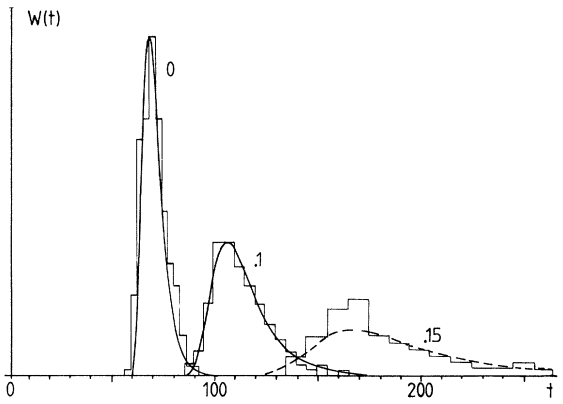

FIG. 7. Delay-time statistics for different depletion rates. Only for strong damping there is noticeable disagreement between the linear (smooth curves) and the nonlinear (histograms) theories.

We also infer from Figs. 5 and 6 that reliable delay-time statistics should be accessible through the early-stage linear theory, provided the limiting intensity $I(\infty)$ obtained from (3.9) is much larger than the maximum intensity implied by the nonlinear theory. We may then use the distribution (2.19) to approximate the probability density of the first-passage time with respect to a reference intensity in the interval

$$1/N \ll I_{\text{ref}} \ll I(\infty) , \tag{3.10}$$

since the normalization integral,

$$\int_0^\infty dt\, W(t) = e^{-I_{\text{ref}}/I(\infty)} - e^{-NI_{\text{ref}}} , \tag{3.11}$$

is sufficiently close to unity for $W(t)$ to reasonably represent the delay-time statistics.

However, if the damping is sufficiently strong, the deviation of the normalization integral (3.11) from unity becomes appreciable. More specifically, for the distribution (2.19) to be applicable we must require

$$1/\Gamma^2 > \langle t_d \rangle_\Gamma . \tag{3.12}$$

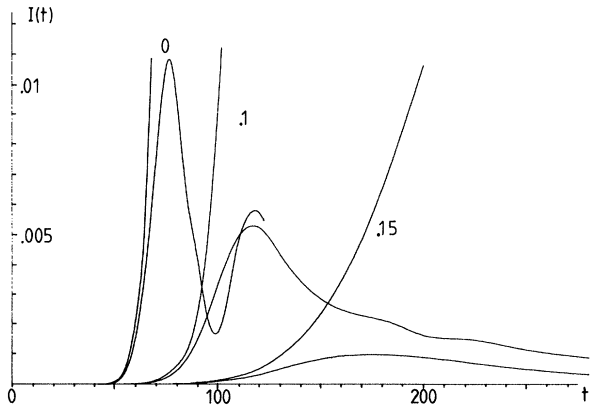

FIG. 6. Comparison of linear and nonlinear trajectories for the mean intensity at the end of the sample for various values of the depletion rate ($\Gamma=0$, 0.1, and 0.15).

Interestingly enough, it is not the linear approximation to the exact dynamics which breaks down when (3.12) is violated. We rather have neither exact nor asymptotic results for the first-passage–time problem. The failure of (2.19) for large Γ is displayed in Fig. 7.

It is instructive to compare the influence of the pumping (discussed in Sec. II) and the depletion (discussed in this section) on the radiation process. Both effects tend to increase the delay and to reduce the radiated intensity. There are, however, characteristic differences, which we show in Fig. 8, for the maximum of the mean intensity and the relative variance of the delay time, and in Fig. 9, for the correlation between the delay time and the intensity maximum. In superfluorescence from fully inverted

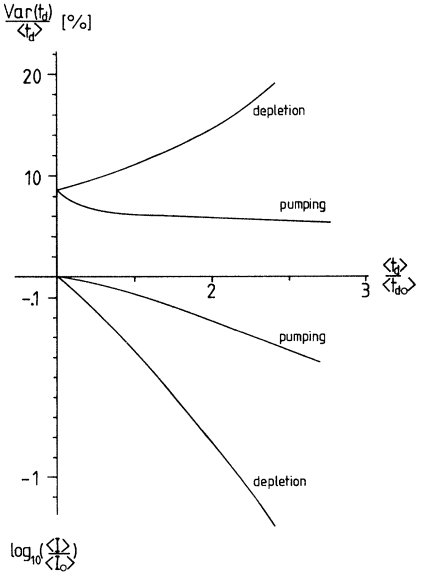

FIG. 8. Effects of pumping and depletion on the delay-time statistics and the mean maximum intensity. The units $\langle t_{d0} \rangle$ and $\langle I_0 \rangle$ refer to the case of no damping and instantaneous pumping. The curves result by varying either the pumping rate γ or the depletion rate Γ.

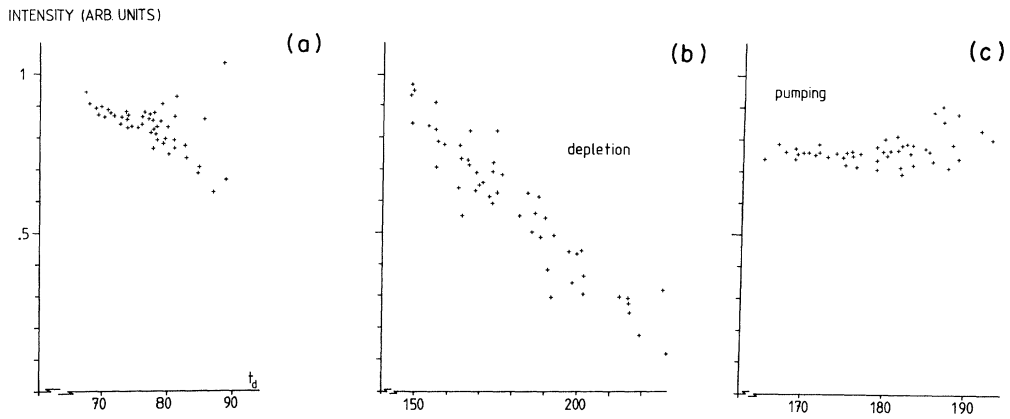

FIG. 9. Effects of damping and depletion on the correlation between delay time and maximum intensity. (a) Instantaneous pumping ($\gamma=\infty$) and no depletion ($\Gamma=0$), (b) instantaneous pumping and finite damping ($\gamma=\infty$ and $\Gamma=0.15$), and (c) slow pumping and no damping ($\gamma=0.006$ and $\Gamma=0$).

two-level atoms there is a slight tendency of "late" pulses to have low maxima [Fig. 9(a)]. This trend becomes much more pronounced if the lower level incurs incoherent depletion [Fig. 9(b)]. For a pumped system without depletion, however, we find this trend completely suppressed [Fig. 9(c)].

IV. TWO-COLOR SUPERFLUORESCENCE IN COMPETITION WITH DAMPING

As our next step towards explaining the Düsseldorf experiment[1] we now consider two optically active level pairs, 32 and 31, which have their upper level, 3, in common. The pair of levels 21 is assumed optically inactive.[6] As an interesting complication we allow for incoherent processes depleting the levels 2 and 1 either independently [see Fig. 10(a)] or in cascade [see Fig. 10(b)]. At any rate, the three-level atoms in question will all be taken to be in the state corresponding to the uppermost level initially.

The pertinent Maxwell-Bloch equations can be written in the following dimensionless forms:

$$\frac{\partial}{\partial t}N_3=-(E_{31}^{+}R_{31}^{+}+E_{32}^{+}R_{32}^{+}+\text{H.c.})\,, \tag{4.1}$$

$$\frac{\partial}{\partial t}N_2=+(E_{32}^{+}R_{32}^{+}+\text{H.c.})-\Gamma_2N_2+\xi_2\,, \tag{4.2}$$

$$\frac{\partial}{\partial t}N_1=+(E_{31}^{+}R_{31}^{+}+\text{H.c.})+[\Gamma_2N_2]-\Gamma_1N_1+\xi_1\,, \tag{4.3}$$

$$\frac{\partial}{\partial t}R_{32}^{\pm}=(N_3-N_2)E_{32}^{\mp}-E_{31}^{\mp}R_{21}^{\mp}-\tfrac{1}{2}\Gamma_2R_{32}^{\pm}+\xi_{32}^{\pm}\,, \tag{4.4}$$

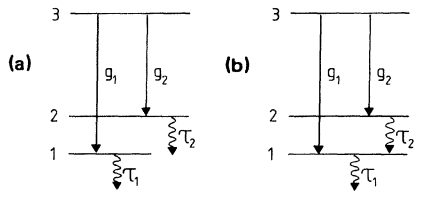

FIG. 10. Level schemes for two-color superfluorescence: (a) independent and (b) cascadic depletion.

$$\frac{\partial}{\partial t}R_{31}^{\pm}=(N_3-N_1)E_{31}^{\mp}-E_{21}^{\mp}R_{21}^{\pm}-\tfrac{1}{2}\Gamma_1R_{31}^{\pm}+\xi_{31}^{\pm}\,, \tag{4.5}$$

$$\frac{\partial}{\partial t}R_{21}^{\pm}=E_{31}^{\mp}R_{32}^{\mp}+E_{32}^{\pm}R_{31}^{\pm}-\tfrac{1}{2}(\Gamma_1+\Gamma_2)R_{21}^{\pm}+\xi_{21}^{\pm}\,, \tag{4.6}$$

$$\frac{\partial}{\partial x}E_{3i}^{\pm}=g_iR_{3i}^{\mp}\quad\text{with } i=1,2\,. \tag{4.7}$$

The term in the square brackets in Eq. (4.3) appears only if the damping mechanisms are in cascade. The coupling constants g_1 and g_2 in the Maxwell equations (4.7) are proportional to the dipole matrix elements for the transitions $3\leftrightarrow1$ and $3\leftrightarrow2$, respectively, and also depend on respective transition frequencies. Since g_1 and g_2 will, in general, be different from one another there is no choice of units for which they both take on the value 1. We shall, however, be interested in the case where $g_1,g_2\approx1$.

The most noteworthy feature in the above field equations is the appearance of the optically inactive polarization component $R_{21}^{\pm}(x,t)$. Owing to the assumed absence of a corresponding dipole matrix element, $R_{21}^{\pm}$ does not give rise to an electric field component $E_{21}^{\mp}$. However, $R_{21}^{\pm}$ has the important effect of coupling the radiated fields $E_{31}^{\pm}$ (the "yellow" pulse) and $E_{32}^{\pm}$ (the "red" pulse). Note that the yellow polarization $R_{31}^{\pm}$ is driven not only by the yellow field $E_{31}^{\mp}$, but also by the red one, $E_{32}^{\mp}$, since the product $E_{32}^{\mp}R_{21}^{\pm}$ corresponds to an oscillation at the yellow frequency as well. Similarly, the product $E_{31}^{\mp}R_{21}^{\pm}$ drives the red polarization $R_{32}^{\pm}$. The red and the yellow pulses are, of course, also coupled by drawing on the same energy reservoir, i.e., the initial population of level 3.

The Langevin forces $\xi(x,t)$ in (4.1)–(4.7) can again be taken to have white spectra, zero means, and Gaussian statistics. We shall have to use

$$\langle\xi_{31}^{\pm}\xi_{32}^{\pm}\rangle=\langle\xi_{32}^{+}\xi_{32}^{+}\rangle=\langle\xi_{31}^{+}\xi_{31}^{+}\rangle=0\,, \tag{4.8}$$

$$\langle\xi_{3i}^{+}(x,t)\xi_{3i}^{-}(x',t')\rangle=\frac{\Gamma_i}{N}\langle N_3(x,t)\rangle\delta(x-x')\delta(t-t')$$

$$\text{for } i=1,2\,.$$

Since the initial state $|0\rangle$ corresponds to full popula-

tion of level 3, we have

$$N_3(x,0)\,|\,0\rangle = |\,0\rangle\ ,\quad N_2(x,0)\,|\,0\rangle = N_1(x,0)\,|\,0\rangle = 0\ , \tag{4.9}$$

and independent Gaussian statistics for the initial polarizations $R_{31}^{\pm}(x,0)$ and $R_{32}^{\pm}(x,0)$ with

$$\langle 0\,|\,R_{3i}^{+}(x,0)R_{3i}^{-}(x',0)\rangle = \frac{1}{N}\delta(x-x') \quad \text{for } i=1,2\ . \tag{4.10}$$

During the early-stage linear regime ($N_3=1, N_{1,2}=0$) the two pulses evolve independently from one another. Both $E_{31}^{\mp}$ and $E_{32}^{\mp}$ are given by (3.8), with appropriate indices on the Langevin forces, the initial polarization operators, and the damping constants. Similarly, the mean intensities $I_{31}\equiv I_{\text{yellow}}$ and $I_{32}=I_{\text{red}}$ can be obtained from (3.9). There are, of course, no cross correlations between the red and yellow pulses in the linear regime.

As soon as the nonlinearities become effective, the two pulses lose their independence. Whichever one of them has grown faster during the preceding linear regime, due to stronger boosts to the random fields $\xi_{31}^{\pm}(x,t)$ and $R_{31}^{\pm}(x,0)$ and/or due to a larger coupling constant g_i, will tend to dominate the other. As the most obvious manifestation of the interdependence we must expect both pulses to have their intensity maxima at times rather close to each other. The maximum values of the two intensities, on the other hand, cannot develop any strong correlation since the partition of the energy between the two pulses is already determined, to a large degree, when their nonlinear coupling sets in.

The above qualitative expectations are indeed borne out by a numerical analysis of the classical versions of the Maxwell-Bloch equations (4.1)—(4.7). In Fig. 11 each cross represents the difference $\Delta t = t_y - t_r$ and the arithmetic mean

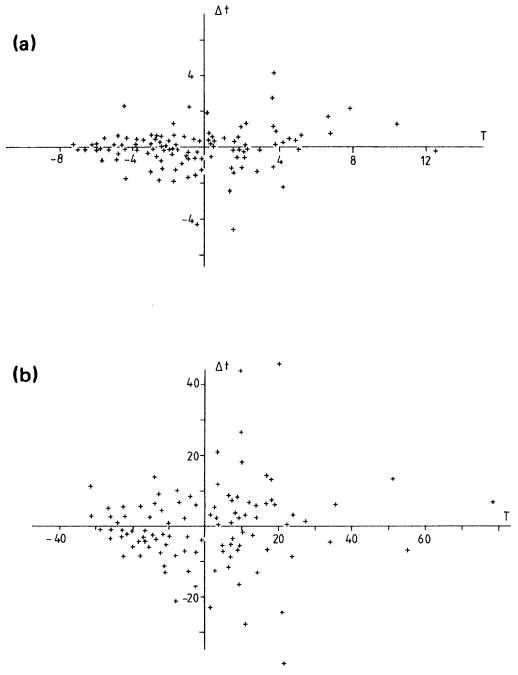

FIG. 11. Difference (Δt) vs mean (T) of the delay times of pulse pairs plotted for (a) undamped systems and (b) the case of independent depletion with $\Gamma=0.15$.

$$T = \tfrac{1}{2}(t_y+t_r) - \tfrac{1}{2}\langle t_y+t_r\rangle$$

of the delay times of the yellow and the red pulses in a single pulse pair. If the two pulses in each pair were independent, the variance of Δt in an ensemble of pulses would be twice the variance of T. The actual cloud of points in Fig. 11 displays, instead, a rather pronounced compression along the Δt axis, and thus indicates a strong tendency towards synchronization of the two pulses in each pair. By comparing Figs. 11(a) and 11(b) we find the synchronization to be impeded by the incoherent depletion process.

Because of the strong coupling mentioned no information on the statistics of the delay-time difference Δt can be gained from a passage-time analysis of the early-stage linear regime. It is a meaningful question, though, whether the fluctuations of the arithmetic mean T of the delay times can be understood within the framework of the linear approximation. As the simplest and most intuitive attempt to answer this question we have studied the statistics of the minimum of the passage times of the intensities $|E_{31}(1,t)|^2$ and $|E_{32}(1,t)|^2$ with respect to suitable reference intensities. By regarding the fields E_{3i} as independent classical processes obeying the linearized versions of (4.4), (4.5), and (4.7), we obtain, using arguments similar to those used to construct (2.19), the distribution function

$$W(t) = W_{31}(t)\int_t^\infty dt' W_{32}(t') + W_{32}(t)\int_t^\infty dt' W_{31}(t')\ , \tag{4.11}$$

where the single-pulse distributions $W_{3i}(t)$ are given by (2.19) with the respective mean intensities $I_{3i}(t)$ as in (3.9),

$$I_{3i}(t) = \frac{g_i^2}{N}\left[1+\int_o^t dt'\, e^{-\Gamma_i t} I_1(2(g_i t')^{1/2})^2/t'\right]\ . \tag{4.12}$$

Performing the time integrals in (4.11) we find

$$W(t) = \frac{I_{\text{ref}}^{(1)}\dot{I}_{31}(t)}{I_{31}(t)^2} e^{-I_{\text{ref}}^{(1)}/I_{31}(t)}\left(1-e^{-I_{\text{ref}}^{(2)}/I_{32}(t)}\right)$$

$$+\,(I_{31}\leftrightarrow I_{32} \text{ and } I_{\text{ref}}^{(1)}\leftrightarrow I_{\text{ref}}^{(2)})\ . \tag{4.13}$$

As reference intensities, $I_{\text{ref}}^{(i)}$, those adopted to their respective one-color calculation should be taken. Note that this result simplifies for the symmetric case in which $\Gamma_1=\Gamma_2$ and $g_1=g_2$.

It is quite rewarding to find that the result (4.13) of the linear analysis agrees well with the histogram of the pair delay obtained from an ensemble of numerical solutions of the nonlinear Maxwell-Bloch equations.

We should note that the clouds in Figs. 11 have been obtained for the case of full symmetry between the two colors, i.e., for independent depletion mechanisms (rather than a cascade) and $\Gamma_1=\Gamma_2$, $g_1=g_2$. The most probable delay-time difference is therefore zero. We have also studied asymmetric cases. The most probable delay-time difference then no longer vanishes. Relatively small differences between the damping constants and/or the coupling constants turn out to shift the $\Delta t - T$ clouds

along the Δt direction quite appreciably. The tendency of one color (the one with the smaller Γ and /or the larger g) to emerge earlier than the other can, incidentally, be understood qualitatively from the linear early-stage analysis.

An interesting asymmetry between the two colors arises even for $\Gamma_1=\Gamma_2$ and $g_1=g_2$ if the damping mechanisms are in cascade. The red pulse then tends to precede the yellow one. For $g_1=g_2=1$ and $\Gamma_1=\Gamma_2=0.15$, we have found $\langle\Delta t\rangle/\mathrm{Var}(\Delta t)\approx-0.25$, a quite sizable shift indeed. The sign of the shift is easily understood from the structure of (4.3). With respect to the case of independent damping mechanisms the cascade tends to fill level 1 and thus to decrease the inversion N_3-N_1 which drives the yellow polarization.

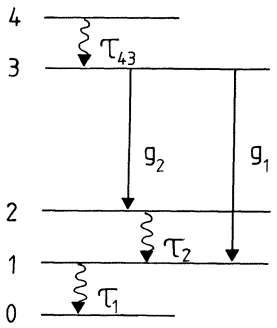

FIG. 12. Level scheme for two-color superfluorescence with pumping and depletion processes.

V. TWO-COLOR SUPERFLUORESCENCE VERSUS DAMPING AND PUMPING

We can now discuss the bearing of our investigation on the experiment performed by Florian, Schwan, and Schmid.[1] We shall be concerned with three features of the observations. (i) One is the joint and rather synchronous appearance, in most shots, of a yellow and a red pulse. The delay time of the pulse pair, in contrast to the delay-time difference for the two pulses in each pair, undergoes large shot-to-shot fluctuations. (ii) There is a range of values for the number density n of initially excited atoms for which the two pulses in a pair tend to be equally intense even though their maximum intensities fluctuate considerably and rather independently. When n is lowered out of this range the red pulse acquires larger intensities than the yellow one, while an increase of n leads to a domination of the yellow pulse. A complete color change takes place as n is varied by about an order of magnitude. (iii) Finally, there is a rather pronounced correlation between the intensity maxima and their delay times: long delays tend to go along with small intensities.

While the three observations just mentioned will find more or less satisfactory explanations below, we shall not discuss a fourth experimental finding, a strong synchronization of the pulse pairs radiated in the forward and in the backward direction.

The simplest level scheme pertinent to the experiment in question is shown in Fig. 12. Initially, level 4, the uppermost one, is the only one populated. Incoherent leakage downwards in energy then fills level 3, from which optical transitions lead to level 2 and level 1. The latter two levels are part of a damping cascade which eventually drains all population towards states irrelevant to the radiation process. The rate constants for the pumping of level 3 and the damping cascades can be controlled, to some degree, by varying the temperature of the surrounding medium. The temperature is sufficiently low (≈ 10 K) for no incoherent upward-in-energy transitions to occur. The number density of initially excited atoms is controlled by the laser pulse used to lift the potentially active atoms from their ground states to level 4.

An attempt to explain the statistics of the measured pulses quantitatively meets with several difficulties. For one, the relaxation times for the pumping (τ_4) and the damping cascade (τ_2 and τ_1) are not known with great precision. Similarly, the natural linewidths $1/\tau_{32}$ and $1/\tau_{31}$ of the optical transitions are not well known. Probably, $\tau_4\lesssim 40$ ps, τ_2 and τ_1 of the order of 100 ps, and τ_{32} and τ_{31} near 2 μs are not unreasonable choices. Absolute values for the number density n are also somewhat uncertain, while relative changes should be under better control. We shall assume n to lie in the range 10^{14}–10^{15} cm^{-3}. There is no uncertainty, of course, about the wavelengths of the red and the yellow transition, $\lambda_{32}=593$ nm and $\lambda_{31}=629$ nm.

The Maxwell-Bloch equations relevant to our five-level system are (4.1)–(4.7) augmented to account for the pumping as in the first two equations in (2.2). The dimensionless rate constants γ, Γ_2, and Γ_1 are related to the times $\tau_{4,2,1}$ as

$$\gamma=\tau_{\mathrm{sf}}/\tau_4\ ,\quad \Gamma_{1,2}=\tau_{\mathrm{sf}}/\tau_{1,2}\ . \tag{5.1}$$

The unit of time appearing here is the so-called superfluorescence time

$$\tau_{\mathrm{sf}}=8\pi\tau/3\lambda^2 ln\ , \tag{5.2}$$

where τ and λ are the mean natural lifetime and the mean wavelength for the two optical transitions, respectively, while l denotes the length of the active volume. It is worth noting that the dimensionless damping constants γ, Γ_2, and Γ_1, as well as the superfluorescence time, are inversely proportional to the number density n.[2]

The dimensionless coupling constants g_i are given by the wavelengths λ_{3i} and the lifetimes τ_{3i} as

$$g_i=\frac{\tau}{\tau_{3i}}\frac{\lambda_{3i}^2}{\lambda^2}\ . \tag{5.3}$$

The observed sychronization of the two pulses within each pair finds its explanation in the results presented in Sec. IV. Even though the pumping of level 3 is not an instantaneous process, it is fast enough for the considerations of Sec. IV to apply quite well. The calculated as well as the measured delay times have the order of 1 ns, while the experimental pumping time is probably shorter than 40 ps. The experiment thus undoubtedly refers to the fast-pumping limit (2.20) rather than the slow-pumping limit (2.21) where the delay times would scale with n as $n^{-1/2}$.

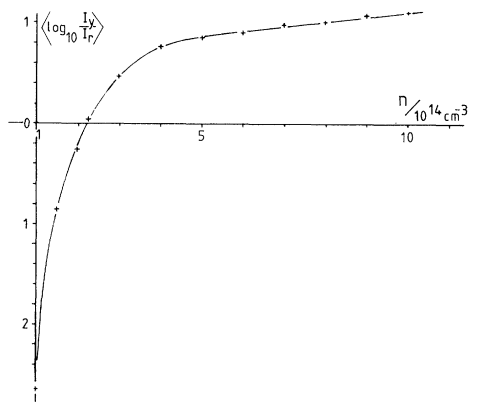

FIG. 13. Color change with varying number density.

The damping cascade, in contrast to the incoherent pump, is of importance for the experiment. Especially, for runs in the low-density limit, the superfluorescence time $\tau_{sf} = \sim 1/n$ becomes so large that the incoherent damping can effectively impede cooperative radiation.

The observed color change can be interpreted as a nonlinear effect, due to the competition of the cooperative radiation with the incoherent damping. We must assume the yellow transition to be favored over the red one by a slightly larger coupling constant,

$$g_1 = 1.1\ , \quad g_2 = 0.9\ , \tag{5.4}$$

but, on the other hand, more strongly impeded by the damping cascade,

$$\tau_1 = 200\ \text{ps}\ , \quad \tau_2 = 400\ \text{ps}\ . \tag{5.5}$$

Since the delay time scales with n as $1/n$, apart from logarithmic corrections,[2] the yellow pulse must dominate for high densities at which the collective radiation develops faster than the damping. For low densities, however, the superfluorescence sets in so slowly that the damping can compete and discriminate against the yellow pulse. Eventually, for sufficiently low n, no superfluorescence of either color can develop any more. The color change is illustrated in Fig. 13 where we show the ratio of the mean maximum intensities for the two colors as a function of the density n.

Finally, the damping cascade is also effective in producing the observed pronounced correlation between long delays and low intensities. Actually, this effect is not exclusive with two-color superfluorescence as can be inferred from Fig. 9. The qualitative remarks at the end of Sec. III apply here as well.

We should add that our calculated ensembles of pulse pairs show a somewhat smaller relative variance of the delay times than was observed experimentally. In the density range from 10^{15} to 10^{14} cm^{-3} we find, using $\tau_{43} = 10$ ps, $\tau = 2\ \mu$s, $\tau_{sf} n = 2.25 \times 10^9$ cm^{-3} and (5.4) and (5.5),[7] the mean delay to grow from 0.4 to 1.2 ns, while the relative variance of the delay increases from 6% to 12%. The experimental variances are larger than ours by about a factor of 5. This discrepancy may well be due to uncontrollable shot-to-shot fluctuations of the density n. The experiment is, after all, performed in a density range rather close to the effective cutoff of superfluorescence by the damping, i.e., in a range where the density enters in a much more sensitive way than in previous experiments on atomic vapors and beams.

ACKNOWLEDGMENTS

We would like to thank our Universität Düsseldorf colleagues R. Florian, L. O. Schwan, and D. Schmid for their infatigable patience in showing us and explaining to us their experiments. We also acknowledge valuable suggestions by Joe Haus and Maciej Lewenstein.

[1](a) R. Florian, L. O. Schwan, and D. Schmid, Solid State Commun. 42, 55 (1982); (b) Phys. Rev. A 29, 2709 (1984).

[2](a) F. Haake, J. Haus, H. King, G. Schröder, and R. Glauber, Phys. Rev. A 20, 2047 (1979); 23, 1322 (1981); (b) D. Polder, M. F. H. Schuurmans, and Q. H. F. Vrehen, J. Opt. Soc. Am. 68, 699 (1978); Phys. Rev. A 19, 1192 (1979).

[3]H. Haken, in *Laser Theory,* Vol. XXV/2C of *Handbuch der Physik,* edited by S. Flügge (Springer, Berlin, 1970).

[4]Note that the pumping we consider is incoherent in nature, in contrast to the one discussed by C. M. Bowden and C. C. Sung, Phys. Rev. Lett. 50, 156 (1983).

[5]M. F. H. Schuurmans and D. Polder, Phys. Lett. 72A, 306 (1979).

[6]F. Haake and R. Reibold, Phys. Lett. 92A, 29 (1982).

[7]As compared to the experiments (Ref. 1) the density range chosen may be too small by roughly 1 order of magnitude. This has been done to achieve numerical convenience. Calculations in a higher-density range would yield similar results provided the relaxation times are suitably changed as well. On the other hand, the number densities quoted in Ref. 1 are upper limits to the actually effective densities [R. Florian, L. O. Schwan, and D. Schmid (private communication)].